Export production and its regulating factors in the West Antarctica Peninsula region of the Southern Ocean

Kuan Huang,[1] Hugh Ducklow,[2] Maria Vernet,[3] Nicolas Cassar,[4] and Michael L. Bender[1]

Received 31 December 2010; revised 25 January 2012; accepted 5 March 2012; published 24 April 2012.

[1] In connection with the Palmer LTER program, mixed layer water samples were collected during the cruise of the L.M. Gould in Jan., 2008 at 49 stations on a 20 × 100 km grid in the West Antarctica Peninsula (WAP) region of the Southern Ocean. In this study, $[O_2]/[Ar]$ ratios and the triple isotope composition of dissolved O_2 were measured, and were used to estimate net community O_2 production (NCP) and gross primary O_2 production (GPP), respectively. These estimates are further converted to carbon export production, primary production and the f-ratio. Our measurements give NCP ranging from −3 to 76 mmol O_2 m^{-2} day^{-1} (−25 to 650 mg C m^{-2} day^{-1}), and GPP from 40 to 220 mmol O_2 m^{-2} day^{-1} (180 to 1010 mg C m^{-2} day^{-1}). The O_2 NCP/GPP ratios range from −0.04 to 0.43, corresponding to *f*-ratios of −0.08 to 0.83. NCP and the NCP/GPP ratio are highest in the northern coastal areas, and decrease to lower values toward the southern coastal area and the open ocean. The inshore-offshore gradient appears to be regulated primarily by iron availability, as supported by the positive correlation between NCP and F_v/F_m ratios ($r^2 = 0.22$, $p < 0.05$). Mixed layer depth (MLD) is inversely correlated with NCP ($r^2 = 0.21$, $p < 0.002$) and NCP/GPP ($r^2 = 0.21$, $p < 0.02$), and highest NCP occurred in the fresh water lenses probably formed from melted coastal glaciers. These results suggest that export production and the f-ratio increase where water stratification is intensified by input of fresh meltwater, and that mixed layer stratification is the major factor regulating NCP in the inner-shelf and coastal regions. Along-shelf variability of phytoplankton community composition is highly correlated with NCP, i.e., NCP increases when the diatom-dominated community in the south transitions to the cryptophyte-dominated one in the north. A high correlation is also observed between NCP and the logarithm of the surface chlorophyll concentration ($r^2 = 0.72$, $p < 0.0001$) , which makes it possible to estimate carbon export as a function of Chl a concentration in this region.

Citation: Huang, K., H. Ducklow, M. Vernet, N. Cassar, and M. L. Bender (2012), Export production and its regulating factors in the West Antarctica Peninsula region of the Southern Ocean, *Global Biogeochem. Cycles*, *26*, GB2005, doi:10.1029/2010GB004028.

1. Introduction

[2] Estimating export production, and understanding its controlling mechanisms, are essential for understanding the global cycles of carbon and other bioactive elements. Previous studies have indicated that export production and the export efficiency (the *f*-ratio, defined by *Eppley and Peterson* [1979]), can be regulated by a wide range of properties, e.g., temperature [*Laws et al.*, 2000], community or food web structure [*Ducklow et al.*, 2001], light [*Hannon et al.*, 2001] and availability of various nutrients [*Pollard et al.*, 2009]. There have also been modeling studies that attempted to estimate export production from surface chlorophyll concentration and ancillary properties [*Dunne et al.*, 2007; *Hidalgo-Gonzalez and Alvarez-Borrego*, 2004; *Iverson et al.*, 2000; *Laws et al.*, 2000]. Ultimately controls on export production need to be examined in a variety of ecosystems spanning a range of forcing properties.

[3] One site of particular interest is the west Antarctica Peninsula (WAP) region of the Southern Ocean, which has been intensively studied in the past two decades by the Palmer Long-Term Ecological Research Project (LTER, *Ducklow et al.* 2007). This polar region consists of a highly productive coastal and continental shelf zone (CCSZ), a relatively productive seasonal ice zone, and a less productive permanently open ocean zone [*Tréguer and Jacques*, 1992; *Ducklow et al.*, 2007]. It thus is characterized by large

[1]Department of Geosciences, Princeton University, Princeton, New Jersey, USA.
[2]The Ecosystems Center, Marine Biological Laboratory, Woods Hole, Massachusetts, USA.
[3]Integrative Oceanography Division, Scripps Institution of Oceanography, University of California, San Diego, La Jolla, California, USA.
[4]Division of Earth and Ocean Sciences, Nicholas School of the Environment, Duke University, Durham, North Carolina, USA.

0886-6236/12/2010GB004028

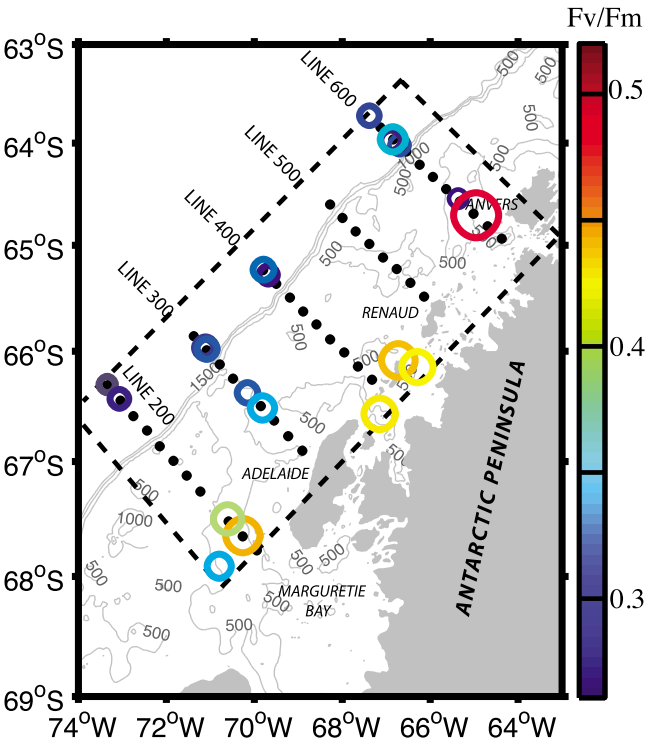

Figure 1. Location of the West Antarctica Peninsula and sampling grid of the cruise Lawrence M. Gould in Jan. 2008. The black dashed line delimits the sampling area, and the black filled dots indicate the stations where samples were collected for analysis of the oxygen properties. The centers of the colorer open circles indicate the locations where variable fluorescence (F_v/F_m) were measured and selected based on the criterion described in the text (section 3.3). The colors and sizes of these circles reflect the magnitude of the F_v/F_m ratios.

seasonal and spatial variability of primary and export production. This region has been surveyed by LTER January cruises since 1993 at a resolution of 100 × 20 km, and a large data set of hydrological and ecological properties have been collected during these cruises [*Ducklow et al.*, 2007]. The observed spatial variability of primary production (PP) is thought to be regulated mainly by the stability of the water column and the nutrient concentrations. *Vernet et al.* [2008] found that PP is enhanced where the water column is strongly stratified as a result of fresh water input from sea-ice and the melting of coastal glaciers. Higher PP was also found where nutrient-enriched upper circumpolar deep water (UCDW) intruded into the inner shelf and mixed up into the surface water there [*Prézelin et al.*, 2000]. Although export production has been measured in the region by a moored sediment trap [*Ducklow et al.*, 2008] and by drifting cylindrical traps and the ^{234}Th method [*Buesseler et al.*, 2010], no studies have measured export production at the same high spatial resolution as other environmental properties.

[4] In samples from the summer cruise in 2008, we made estimates of export production and the *f*-ratio by utilizing properties of dissolved O_2 in mixed layer water samples collected at each grid station. The isotopic composition of dissolved O_2 in the mixed layer gives a measure of the fraction of dissolved O_2 derived *in situ* from photosynthesis [*Luz and Barkan*, 2000]. The O_2 supersaturation in excess of argon (Ar) supersaturation reflects biological supersaturation of O_2 [*Reuer et al.*, 2007]. These anomalies with respect to air saturation values are maintained by gross primary O_2 productivity (GPP) and respiration (R), and reflect the rate of GPP and net community O_2 productivity (NCP). GPP can be calculated from the isotope anomaly and gas transfer velocity (estimated from a wind speed parameterization). The net flux of biological O_2 to the atmosphere, calculated from the O_2 supersaturation in excess of Ar and the gas exchange velocity, equals NCP. Since storage of organic carbon in the mixed layer is modest with respect to NCP [*Ducklow et al.*, 2007], NCP approximates carbon export production [*Falkowski et al.*, 2003].

[5] Our work thus gives new high resolution maps of export production and the f-ratio. In this paper, we report these results, and analyze the correlation of the productivity with other environmental and ecological properties, e.g., sea surface temperature (SST), mixed layer depth (MLD), nutrients, and phytoplankton community composition. Through these relationships, we examine the major factors regulating export production in the region, and test hypotheses about the mechanisms through which environmental factors control carbon export.

2. Methods

2.1. Sampling Strategy and Hydrological Data

[6] The Palmer LTER sampling grid stretches 900 km alongshore, with 10 transect lines (No. 000-900), 100 km apart, perpendicular to the WAP. Each of these transect lines has about 10 stations which are spaced 20 km apart (Waters and Smith, 1992). The 2008 cruise spanned five transect lines (No. 200-600, see Figure 1) and covered about 50 stations in the grid from Jan. 6–29, climatologically a period of high carbon flux in the annual cycles according to the long-term sediment trap data [*Ducklow et al.*, 2008]. A pair of surface samples for analysis of dissolved O_2 properties, together with samples for macro-nutrient profiles, pigment profiles, etc., were collected at each station. Conductivity-temperature-depth (CTD) profiles and oxygen concentration profiles were measured at the stations, and temperature, salinity, oxygen, and variable fluorescence (F_v/F_m) were measured underway. Mixed layer depth was taken as the depth where the absolute difference of potential temperature to the surface ($\Delta\theta = |\theta_0 - \theta_d|$) = 0.2°C [*Dong et al.*, 2008]. Euphotic zone depth (Z_{eu}) was determined where PAR was 1% of the surface value.

2.2. O_2 NCP and GPP

[7] A pair of mixed layer water samples, 150 to 350 ml in volume, were collected and stored in pre-evacuated and pre-poisoned flasks. The dissolved O_2/Ar ratios and the triple oxygen isotopic compositions ($^{16}O/^{17}O/^{18}O$) were measured on a Finnigan Delta Plus XP or a Finnigan Mat 252 Dual Inlet Mass Spectrometer. The detailed methods for sample collection and analysis are summarized by *Hendricks et al.* [2004] and *Reuer et al.* [2007]. Using the gas exchange rate parameterized from wind speed, the O_2/Ar ratios are

converted to NCP and the triple oxygen isotopic compositions are converted to GPP, following the approach described by *Quay et al.* [1993], *Luz and Barkan* [2002], and *Hendricks et al.* [2004], using the numerical method of *Reuer et al.* [2007]. These methods assume a constant MLD and productivity over the period of about 1 week prior to the sample collection, and they assume that there is no significant vertical exchange of water across the bottom of the mixed layer. They involve wind speeds and the gas transfer velocity parameterized in terms of wind speed [*Reuer et al.*, 2007; *Sweeney et al.*, 2007].

2.2.1. $\Delta(O_2/Ar)$ and NCP

[8] O_2 and Ar have similar solubilities. While Ar is conservative with respect to biological processes, O_2 saturation is altered by photosynthesis and respiration. Thus, Ar can correct for physical saturation due to warming, bubble entrainment, mixing and atmospheric pressure variations. The deviation of the O_2/Ar ratio from its saturation concentration ratio is defined as:

$$\Delta(O_2/Ar) = \left[\frac{(O_2/Ar)_{sample}}{(O_2/Ar)_{sat}} - 1\right] \times 100\% \quad (1)$$

This term represents the biological O_2 supersaturation. NCP is then calculated as:

$$NCP = k\rho[O_2]_{sat}\Delta(O_2/Ar), \quad (2)$$

where ρ is the density of the surface water, and k is the gas exchange rate. NCP, in units of mmol O_2 m^{-2} day^{-1}, stands for daily averaged the air-sea flux of O_2 over a period of up to several weeks [*Reuer et al.*, 2007], and can be converted to carbon NCP using O_2/C = 1.4 [*Laws*, 1991].

2.2.2. Triple Oxygen Isotopic Composition and GPP

[9] The isotopic composition of dissolved oxygen is reported in the δ notation, but in units of per meg (part per million) rather than per mil, i.e.,

$$\delta^* O = \left[\frac{(^*O/^{16}O)_{sample}}{(^*O/^{16}O)_{standard}} - 1\right] \times 10^6 \text{ per meg}, \quad (3)$$

where * denotes for the heavier isotopes, i.e., ^{17}O and ^{18}O. The standard used here is atmospheric oxygen. $\delta^{17}O$ and $\delta^{18}O$ of dissolved O_2 vary with several processes, i.e., photosynthesis, respiration and gas exchange. The degree of mass-independent fractionation is:

$$^{17}\Delta \approx \delta^{17}O - 0.518 \times \delta^{18}O \text{ per meg} \quad (4)$$

where 0.518 is the coefficient associated with the mass-dependent fractionation [*Luz and Barkan*, 2009]. Dark respiration introduces mass-dependent fractionation of ^{17}O and ^{18}O in a steady state so that $^{17}\Delta$ is not altered by respiration [*Angert et al.*, 2003]. By contrast, photosynthesis adds O_2 with $^{17}\Delta$ of 249 per meg [*Luz and Barkan*, 2000], which is identical to the oxygen isotopic composition of seawater. Gas exchange shifts $^{17}\Delta$ toward 8 per meg [*Reuer et al.*, 2007], the value in equilibrium with air O_2 (which by definition has $^{17}\Delta = 0$). Thus, $^{17}\Delta$ reflects the fraction of dissolved oxygen produced by photosynthesis. $^{17}\Delta = +8$ per meg when all O_2 is dissolved atmospheric O_2, and +249 per meg when all dissolved O_2 comes from photosynthesis. In a system at steady state, GPP can be estimated by the approximation given by *Hendricks et al.* [2004]:

$$GPP \approx k\rho[O_2]_{sat}\frac{^{17}\Delta_{Sat} - ^{17}\Delta_{Diss}}{^{17}\Delta_{Diss} - ^{17}\Delta_W} \quad (5)$$

where $^{17}\Delta_{Sat} = 8$ per meg, $^{17}\Delta_W = 249$ per meg and $^{17}\Delta_{Diss}$ is the measured value of a sample.

[10] O_2 GPP can be converted to ^{14}C PP, using the ratio of gross O_2 production/^{14}C PP of 2.7 diagnosed by *Marra* [2002]. At steady state, and assuming the production rate of dissolved organic carbon (DOC) is much smaller than NCP, carbon NCP is approximately equal to particulate carbon export production, and O_2 NCP/GPP is about half of the *f*-ratio defined by *Eppley and Peterson* [1979].

2.2.3. Gas Exchange Rate (k)

[11] Daily 10 m wind speeds from the NCEP/NCAR reanalysis [*Kalnay et al.*, 1996] are used to calculate the gas transfer velocity (piston velocity) following the formula of *Sweeney et al.* [2007]. As the O_2 concentration of the samples is dependent on the gas exchange history of the surface water, a weighting technique is used to account for the variability of wind speed and gas transfer velocity during 60 days prior to the date the samples were collected (see *Reuer et al.* [2007] for details). Therefore, the k values calculated from this method represent the weighted average of the influence of wind speeds in the past two months, weighted heavily to the week or so before samples were collected.

[12] Wind speeds were measured on the cruise with an R.M. Young sensor on the vessel, and were converted to true wind speeds. A systematic bias of NCEP/NCAR wind speed from the daily average of the true wind speed is observed (Figure S1 in the auxiliary material).[1] Linear regression analysis gives: true wind speed (m s^{-1}) = 1.0 × NCEP/NCAR wind speed + 2.8 (m s^{-1}), $r^2 = 0.63$, n = 39.

[13] The bias is also observed by comparing daily average wind speed measured at Palmer Station and the NCEP/NCAR wind speed from 2000–2010 (Figure S1), with measured wind speed (m s^{-1}) = NCEP/NCAR wind speed (m s^{-1}) + 3, $r^2 = 0.28$, n = 3731.

[14] The bias observed in these comparisons indicates that NCEP/NCAR reanalysis tends to underestimate wind speed consistently in the study region. The regression equation relating wind speeds measured on board the ship to NCEP/NCAR values is thus used to correct for the wind speed.

2.3. Nutrients, Chlorophyll, and Other Plant Pigments

[15] Samples for dissolved inorganic nutrients (nitrate, phosphate and silicate) were analyzed following in-line filtration through GF/F filters and frozen storage (−20°C). Nutrient concentrations were determined by standard flow infection analysis protocols using a Lachat QuikChem 8000 (Lachat Instruments Div., Zellweger Analytics, Inc. Loveland, CO).

[16] Concentration of chlorophyll a was estimated fluorometrically. Seawater aliquots were filtered though Millipore HA filters, the filters extracted in 90% acetone and stored frozen for 24 h [*Smith et al.*, 1981]. Concentrations of

[1] Auxiliary materials are available in the HTML. doi:10.1029/2010GB004028.

pigments in acetone were measured using a digital Turner Designs fluorometer that was calibrated with pure Chl a dissolved in 90% acetone.

[17] Phytoplankton pigments were determined using High-Performance Liquid Chromatography (HPLC) as follows. Filters were extracted in 90% grade acetone and ultra-sonicated while held in a −20°C bench-top cooler for 10 seconds, stored at −80°C for 24 hours and pre-filtered through a 0.45 μM Whatman nylon Pradisk filters before injection. Samples were separated using an Agilent Technologies (Hewlett-Packard) 1100 Series HLC system, equipped with G1314A variable wavelength (fixed at 440 nm), G1315A diode array (scanning 330–800 nm) and G1321A fluorescence (440 nm excitation, 650 nm emission) detectors. Solvents were degassed using a vacuum degasser and column temperature was maintained at 25°C with a G1316A column thermostat. Agilent Technologies ChemStation for LC 3D software was used for system control and data collection and peaks were quantified at 440 nmM on the VWD. Further details are given by *Kozlowski* [2008].

2.4. Phytoplankton Community Structure

[18] Using the CHEMTAX program [*Mackey et al.*, 1996], average accessory pigment concentrations in the mixed layer determined by HPLC were used as chemotaxonomic markers to reconstruct the phytoplankton community composition in the mixed layer of the WAP region. With an initial matrix of accessory pigments to Chl a ratios in the major phytoplankton groups, CHEMTAX uses factor analysis and a steepest descent algorithm to optimize the pigment ratios, and calculates the contribution of each group to total Chl a [*Mackey et al.*, 1996, 1998]. To run CHEMTAX program in this study, we used a localized "wAP" method that has been validated by long-term HPLC data set (1995–2007) collected in the WAP region [*Kozlowski et al.*, 2011]. As described by *Kozlowski et al.* [2011, Table 5], this method uses a initial pigment ratio matrix that includes 6 accessory pigments (chlorophyll c2, fucoxanthin, 19′ butanoyloxyfucoxanthin , 19′ hexanoyloxyfucoxanthin, alloxanthin andchlorophyll b) in 5 representative phytoplankton groups in the study region (diatoms, cryptophytes, type 4 haptophytes, mixed flagellates, and prasinophytes). The configuration parameters for the CHEMTAX run were identical as listed by *Kozlowski et al.* [2011]. In particular, the ratio limits for the run was set to 500, which allowed the program to modify the pigment ratio (r) from r/6 to 6r.

2.5. Sea Ice Extent

[19] The 25 × 25 km sea ice concentration data, generated from the Nimbus-7 SSMR and DMSP SSM/I Passive Microwave [*Fetterer et al.*, 2007], were retrieved from the National Snow and Ice Data Center, University of Colorado, Boulder Colorado. Following the method described by *Stammerjohn et al.* [2008], these data are used to determine the time that a station was free of sea ice before it was occupied on the cruise.

3. Results

[20] Major results of this study are summarized in Table S1.

3.1. Hydrography

[21] The hydrographic structure of the upper water column in Jan. 2008 was similar to that described by *Klinck et al.* [2004] and *Smith et al.* [1999]. Generally, the surface water had a potential temperature (θ) > 0°C and salinity <34 per mil. This layer represented the summer Antarctic Surface Water (AASW). The low salinity of this water reflects the influence of sea-ice and coastal glacier meltwater [*Dierssen et al.*, 2002; *Smith et al.*, 1999; *Vernet et al.*, 2008]. A 50–100 m thick layer with higher salinity (33.8 to 34.2) and lower θ (0 to −1.5°C) was present below the summer AASW . The coldest (T_{min}) water was the remnant of winter water(WW) that had been cooled to the freezing point during the previous winter. Its core usually lay around 80–100 m. Below 100 m, the cold WW transitioned to the warmer and saltier UCDW intrusion, with $0.5 < \theta < 2$°C and salinity >34.6 per mil [*Prézelin et al.*, 2000].

[22] The absence of core WW deserves at some places a closer examination. In the northern coastal region, the potential temperature at the depth of the temperature minimum ranged from −0.8 to 0.3°C, much higher than the upper limit of WW temperature (−1.2°C) suggested by *Martinson et al.* [2008] (Figure 2a). Salinity at the T_{min} layer in this region was >34.2, also greater than the upper limit (34.13) given by *Martinson et al.* [2008] (Figure 2b). The high temperature and salinity observed at the T_{min} layer in this region suggest intense vertical mixing with both surface water above and modified UCDW below, which may have been brought to the WW depth by upwelling [*Smith et al.*, 1999; *Prézelin et al.*, 2000].

[23] Sea surface temperature (SST) in the coastal and inner shelf areas was high (>1.5°C) compared with that offshore (Figure 2c). In contrast, sea surface salinity (SSS) showed less variability in most of the region, except to the southwest of the Anvers Island where salinity was extremely low (Figure 2d).

[24] Upper water column stratification was strengthened by the input of fresh sea-ice and coastal glacier meltwater. The mixed layer in the WAP region was generally shallow, with a mean depth for all stations of 24 ± 10 m (Figure 2e). Hydrographic data along lines 300–600 indicated a MLD 20–30 m deep, with the bottom of the mixed layer tilting slightly downward from onshore to offshore. In places where there was a warmer and fresher water lens, the water column was more strongly stratified and the MLD was shallower than 10 m. Along line 200, where there was no fresh water patch in the surface, the mixed layer was deep (∼50 m) in the nearshore area, and shoaled to ∼35 m toward offshore. MLDs along this line were the deepest in the study region.

[25] The depth of the euphotic zone (z_{eu}) ranges from 25–94 m over the region, with a mean of 59 ± 16 m. The euphotic layer was thinnest in the northern shelf and coastal regions (line 200–300), and thickened toward the southern region and the offshore region. z_{eu} exceeded the MLD over the region, with the mean z_{eu}-MLD = 37 ± 16 m. As shown in Figure 2f, absorbed PAR in the mixed layer (PAR_{MLD}) accounts for 51–91% (mean = 80 ± 11%) of the total PAR in the euphotic zone (PAR_{eu}). The distribution of PAR_{MLD}/PAR_{eu} indicates that our estimates of NCP and

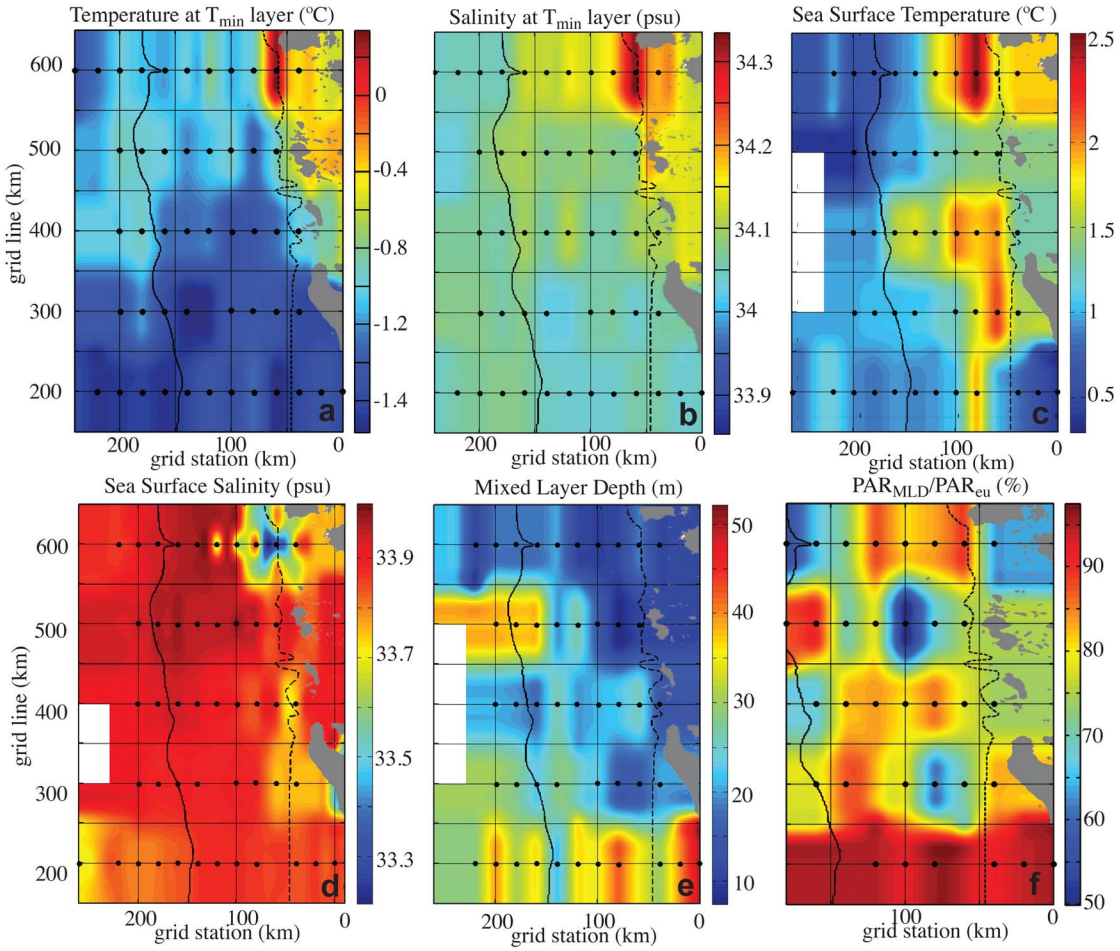

Figure 2. (a) Potential temperature and (b) salinity at the depth of temperature minimum (T_{min}), (c) sea surface temperature (SST), (d) sea surface salinity (SSS), (e) mixed layer depth (MLD), and (f) the ratio of integrated PAR in the mixed layer to that in the euphotic zone for Jan. 2008 in the Palmer LTER grid. The dark line shows the location of shelf break, and the dashed line shows the western boundary of the coastal area. Area between the two lines is referred as shelf area in the text. Black dots indicate locations where samples were collected. Grid Station 0 (km) is in the vicinity of the inshore boundary of the study region shown in Figure 1.

GPP represent a major fraction of euphotic zone productivity over most of the study region.

3.2. Nutrients

3.2.1. Surface Nutrient Concentration

[26] Concentrations of macro-nutrients in the surface water were generally high. The phosphate concentrations ranged from 0.6 to 2.2 mmol m^{-3}, with a mean of 1.5 ± 0.2 mmol m^{-3}. Concentrations were higher offshore, and decreased to lower values in coastal areas (Figure S3a). Concentration less than 1 mmol m^{-3} occurred only in Marguerite Bay (inshore part of line 200), where PP and chlorophyll are usually high in austral summer [*Ducklow et al.*, 2007]. By contrast, silicate concentrations were higher inshore, with peak values of 87 mmol m^{-3}, and decreased toward the open sea to as low as 27 mmol m^{-3} (Figure S3b). Although large variability existed, the range of surface nutrient concentrations indicate that macro-nutrients are unlikely to limit productivity in this region.

3.2.2. Integrated Nutrient Uptake

[27] Following the methods of *Serebrennikova and Fanning* [2004], depth-integrated drawdown of macro-nutrients were calculated as the sum of decrease of nutrient concentration above the core of the remnant of winter water (WW), i.e., the depth of minimum temperature. This method assumes that surface water down to 100–150 m was homogeneous in winter, and nutrient concentrations at the core of the WW have not varied significantly during the growth of phytoplankton in spring and summer [*Klinck et al.*, 2004; *Serebrennikova and Fanning*, 2004].

[28] Phosphate drawdown (ΔP, ranging from 7 to 40 mmol m^{-2}) in the shelf area had the highest mean (24 ± 6 mmol m^{-2}), while the average ΔP in the coastal and the offshore areas were 20 ± 6 and 18 ± 8 mmol m^{-2},

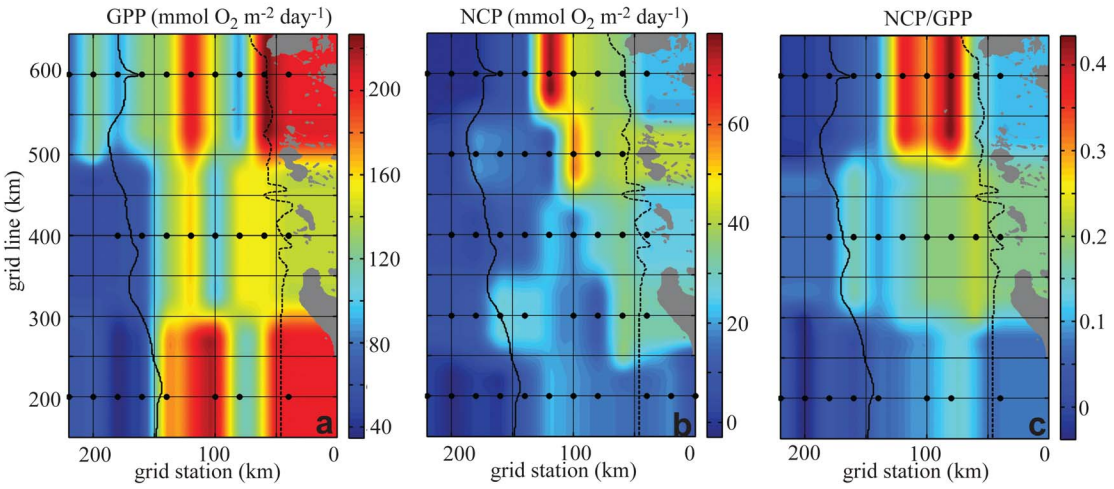

Figure 3. (a) Gross primary production (GPP), (b) net community production (NCP), and (c) NCP/GPP ratio for Jan. 2008 in the Palmer LTER grid. Note that there are no GPP and NCP/GPP data on line 300 and 500, and the interpolations used in Figures 3a and 3c are mainly intended to show the values and trends of GPP and NCP/GPP ratios on line 200, 400 and 600.

respectively. The largest ΔP occurred in the northern inner shelf and coastal areas (Figure S3c).

[29] Silicate drawdown (ΔSi) varied by nearly a factor of 9 from 190 to 1700 mmol m^{-2}, considerably more than that of ΔP. ΔSi was higher in the open sea (with the mean of 730 ± 360 mmol m^{-2}) and decreased toward the coast (with the mean of 630 ± 290 and 470 ± 280 mmol m^{-2}, respectively, in the shelf and coastal areas). Thus, it showed a trend which was inverse to that of ΔP (Figure S3d).

3.3. Photosynthetic Competency (F_v/F_m)

[30] Iron concentrations in the WAP region have been reported only by *Martin* [1990], who measured iron concentrations (7.4 nmol kg^{-1}) during late summer of 1989 in surface water of the Gerlache Strait east of Anvers Island. As an alternative, the photosynthetic competency (F_v/F_m) of Photosystem II (PSII) of the surface water phytoplankton was measured for Jan. 2008. The measured F_v/F_m varied from 0.26 to 0.56, with a mean of 0.39 ± 0.08 (n = 20). Strong diurnal signals were observed in most of the measurements, with peak values occurring in the dawn and strong depression of the ratios at noon as a result of intensive photo inhibition of the phytoplankton in surface water. To eliminate the imprint of diurnal signals on the spatial variations, we selected F_v/F_m within a limited range of photosynthetically active radiation (PAR). Our PAR window corresponds to the raw values of 0 to 200 mV measured by the PAR sensor (Figure S2). It encompasses the period from midnight to ~4 a.m. local time when F_v/F_m ratios increased from the dark condition to ward the maximum values. An average value of these selected F_v/F_m ratios in one day is calculated and applied to stations occupied during hours of the measurement window. The calculated F_v/F_m decreased from inshore to offshore, with average values of 0.41 ± 0.03, 0.37 ± 0.1 and 0.30 ± 0.03 in the coastal, shelf and offshore areas, respectively (Figure 1). F_v/F_m in the shelf area decreased from north to south, with high values around 0.5 occurring about 20 km to the southwest of Anvers Island.

3.4. O_2 Properties and Production

3.4.1. $^{17}\Delta$ and the O_2 GPP

[31] Sample pairs from 26 stations on lines 200, 400 and 600 were analyzed concurrently for both $^{17}\Delta$ and $\Delta(O_2/Ar)$, and samples from another 20 stations on line 300 and 500 were analyzed only for $\Delta(O_2/Ar)$ (Figure 5a).

[32] The $^{17}\Delta$ ranged from 17 to 72 per meg, with a mean of 43 ± 15 per meg. The precision of the measurements is quantified by the agreement of measurements of a pair of samples on each station. In this study, the root mean square (RMS) deviation from the mean of the sample pairs was ±5 per meg, corresponding to the population standard deviation of ±7 per meg.

[33] The gas exchange coefficient (k) calculated from the wind speed was in the narrow range of 2.3 to 2.9 m day^{-1}. Using these k values in equation (5) gives the GPP in this region from 40 to 220 mmol O_2 m^{-2} day^{-1} (Figure 3a). According to the photosynthetic quotient given by *Marra* [2002], O_2 GPP approximates 2.7 × ^{14}C production. Therefore, our estimates of O_2 GPP are equivalent to ^{14}C productivity of 180–1010 mg C m^{-2} day^{-1}.

[34] There was a clear cross-shelf trend of the GPP distribution. The average GPP was highest in the coastal area (180 ± 40 mmol O_2 m^{-2} day^{-1}, n = 3), high in the shelf (150 ± 50 mmol O_2 m^{-2} day^{-1}, n = 13), and much lower offshore (90 ± 40 mmol O_2 m^{-2} day^{-1}, n = 10). In the inner-shelf and coastal areas, GPP was similarly high in the southern and northern lines (200 and 600), while it was slightly lower in the central part (line 400).

3.4.2. $\Delta(O_2/Ar)$ and the O_2 NCP

[35] For all stations, $\Delta(O_2/Ar)$ varied from −0.3 to +10.9 %. The mean $\Delta(O_2/Ar)$ was 2.5 ± 2.4%. $\Delta(O_2/Ar)$ was ≥0, within the measurement error, for all samples, indicating that mixed layer water in this region was dominantly autotrophic. The RMS deviation from the mean of duplicates was ±0.27%, and the population standard deviation is 0.37%. NCP calculated from these measurements and the k values ranged from −3 to 76 mmol O_2 m^{-2} day^{-1}

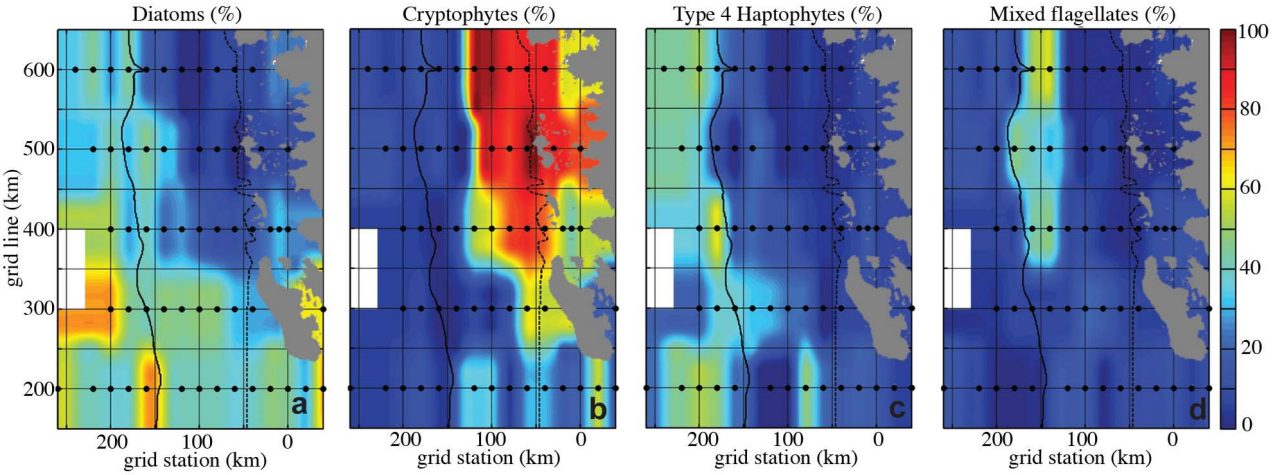

Figure 4. Contribution (%) of (a) diatoms, (b) cryptophytes, (c) type 4 haptophytes, and (d) mixed flagellates to total Chl *a* in the surface water derived from the HPLC-CHEMTAX analysis for Jan. 2008 in the Palmer LTER grid.

(Figure 3b), or −25 to 650 mg C m^{-2} day^{-1} when applying the O_2 NCP:Carbon NCP stoichiometry of 1.4 given by *Laws* [1991].

[36] GPP explains 39% of the variance in NCP (Figure 5b). The sense of the relationship is as expected: NCP are higher where GPP is higher. However, while GPP decreased from the coastal to the open sea areas, the spatial variation of NCP was more complicated. NCP was highest on average in the shelf area (27 ± 15 mmol O_2 m^{-2} day^{-1}, n = 26) and had the largest variation. The average rate of NCP and its variance were less in the coastal area (20 ± 8 mmol O_2 m^{-2} day^{-1}, n = 6). NCP in the open sea area was consistently low at the time of our observations (3 ± 5 mmol O_2 m^{-2} day^{-1}, n = 14). The large variation of NCP in the shelf area was mainly due to an along-shore gradient; i.e., NCP was much greater in the northern shelf than in the south. Highest NCP was found in the mid-shelf along line 600, about 50 km to the west of Anvers Island.

[37] NCP is highly correlated with $\Delta(O_2/Ar)$ (n = 46, r^2 = 0.96, p < 0.0001), while much less correlated with the gas exchange rate (n = 46, r^2 = 0.25, p < 0.0005). Therefore, the uncertainty in the estimates of wind speed and calculation of the gas exchange rate will not significantly affect the variability of NCP estimated by our method.

3.4.3. NCP/GPP Ratios and the *f*-Ratios

[38] O_2 NCP/GPP ratios measured at 26 stations ranged from −0.04 to 0.43 (Figure 3c). Using O_2/C = 1.4 and O_2 GPP/^{14}C PP = 2.7, the *f*-ratio is about two times the O_2 NCP/O_2 GPP ratio. Thus, *f*-ratios in the regionranged from nearly 0 to 0.83.

[39] The variance of NCP accounts for most of variance in NCP/GPP ratios (r^2 of NCP and NCP/GPP = 0.9, n = 26, p < 0.0001), and the spatial distribution of NCP/GPP is similar to that of NCP. NCP/GPP ratios in the shelf area were generally high and variable (0.20 ± 0.11). Ratios in the coastal region and open sea were lower (mean = 0.12 ± 0.05 and 0.02 ± 0.03, respectively). Similar to that of the NCP, NCP/GPP was highest in the northern coastal region, and was lower in the southern coastal region.

3.4.4. Uncertainties of the Estimates

[40] Uncertainties in the calculated values of NCP and GPP mainly arise from uncertainties in the gas exchange coefficient and the analytical uncertainties of the $\Delta(O_2/Ar)$ and the $^{17}\Delta$. The standard error of ±0.27% in the $\Delta(O_2/Ar)$ measurements is ±11% of the mean $\Delta(O_2/Ar)$ value. The standard error of ±5 per meg corresponds to an uncertainty of ±2% in mean photosynthetic O_2 concentration. Using the average saturation [O_2] of 350 mmol m^{-3} and the average *k* of 2.3 m day^{-1} over the study region, these standard errors give the uncertainties of ±2 mmol O_2 m^{-2} day^{-1} and ±3 mmol O_2 m^{-2} day^{-1} in NCP and GPP, respectively.

[41] According to *Sweeney et al.* [2007], the wind speed parameterization we adopted in this study gives an uncertainty of ±32% in the gas transfer velocity. Combining this error with the analytical uncertainties yields an overall uncertainty of ±34% (±5 mmol O_2 m^{-2} day^{-1}) in NCP, and ±33% (±40 mmol O_2 m^{-2} day^{-1}) in GPP.

[42] The error analysis indicates that the major fraction of the uncertainties in NCP and GPP is from the error in the gas exchange rate calculation. As *k* is eliminated in the calculation of the NCP/GPP ratios, our NCP/GPP have a considerable smaller uncertainty (±12%, or 0.02 in NCP/GPP).

3.5. Community Structure

[43] Distribution of phytoplankton composition in the mixed layer is presented in Figure 4. The CHEMTAX run gave an root mean square error (RMSE) of 3.4%, which is smaller than the average of the uncertainties (8.0 ± 5.4%) in the CHEMTAX calculations for the 12 year data set [*Kozlowski et al.*, 2011].

[44] Diatoms and cryptophytes contributed significantly to the total Chl a in the WAP region. The contribution of diatom (f_{diat}) ranged from 0 to 71%, with the mean = 31 ± 18% (n = 45) . Diatoms were dominant in most of the offshore areas and the southern coast and shelf areas, and had high contribution in Marguerite Bay (Figure 4a). In the northern shelf and coastal areas, the fraction of diatom chlorophyll was generally less than 10%.

[45] Cryptophytes accounted for 0 to 97% of the contribution to total Chl a (mean of f_{cryp} = 34 ± 35%). They were dominant in the coast and shelf areas north of line 300, and were most important in the inner-shelf of line 500 and 600 (Figure 4b).

[46] Type 4 haptophytes are primarily represented by *Phaeocystis antarctica* in this region [*Kozlowski et al.*, 2011], and they were less dominant compared with diatoms and cryptophytes (f_{hap} from 0 to 59 %, mean = 20 ± 17%). They have relatively high contribution west of the shelf break (Figure 4c).

[47] The mixed flagellates had low contribution to total Chl a in most of the study region (f_{mix} from 0 to 57 %, mean = 13 ± 15%), except in a narrow area (about 20 km wide) to the east of the shelf break and to the north of line 300 (Figure 4d).

[48] Prasinophytes contributed least to the total Chl a, and were hardly identified in the study region (f_{pra} from 0 to 14 %, mean = 2.5 ± 3.8%).

[49] Although there may be considerable inter-annual variability and additional uncertainty due to different methods, phytoplankton composition derived from the HPLC-CHEMTAX analysis for Jan. 2008 in this region is quite comparable to that observed in previous studies using similar methods or microscopic analysis. These studies all observed high abundance of diatoms and cryptophytes relative to other groups in the region, with cryptophytes dominating only in the northern inshore area [*Garibotti et al.*, 2003; *Moline et al.*, 2004; *Kozlowski et al.*, 2011].

4. Discussion

[50] Previous studies have identified two major factors that are key to the ecosystem structure and dynamics in the WAP region. The first is sea-ice and coastal glacier runoff. Supply of fresh water during sea-ice retreat and melting of glaciers enhances the strength of upper water column stratification, and thus, the availability of light to phytoplankton in the mixed layer [*Dierssen et al.*, 2002; *Smith and Nelson*, 1986; *Buesseler et al.*, 2003]. In a 12 year time series (1995–2006) analysis, *Vernet et al.* [2008] observed that primary productivity is higher where the mixed layer is shallower. In addition, warmer and fresher water lenses originating from glacier melt are usually favored by cryptophytes. Glacier meltwater can thus shift community composition and alter the food web, and could potentially regulate productivity [*Moline et al.*, 2004].

[51] The second important process in this region is the intrusion of UCDW into the shelf, which supplies nutrients to the surface water by vertical mixing and upwelling, and enhances primary productivity [*Prézelin et al.*, 2000, 2004; *Garibotti et al.*, 2003].

[52] Although these processes play an important role in regulating primary productivity, it is still unclear how they influence export productivity in this region. With our estimates of NCP, NCP/GPP and the environmental and ecological properties, we carried out Type I linear regression analyses and examined the role of several factors in regulating NCP and export efficiency. Although linear relationships were assumed for the calculation, we focused on the trends of relationships rather than the exact functionality relationships between NCP and the environmental properties. r^2 and p were used as indication of the strength of the trends.

4.1. Influence of Water Column Stratification

[53] As mentioned above, warming and freshening of the surface water in the coast and shelf areas was a result of fresh water supply from sea-ice retreat and melting of coastal glaciers. This supply accounts for the formation of a shallow mixed layer [*Smith and Nelson*, 1986]. Correlation analysis between NCP and environmental properties indicates that NCP was positively correlated with SST (n = 46, r^2 = 0.36, p < 0.0001, see Figure S4a), and inversely correlated with MLD (n = 46, r^2 = 0.21, p < 0.002, see Figure 5c). A similar relationship was observed between MLD and the NCP/GPP ratio (n = 26, r^2 = 0.21, p < 0.02, see Figure 5d), and between MLD and the volumetric NCP, i.e., NCP/MLD (Figure S4b).

[54] The correlation study suggests that strengthening of mixed layer stratification and shoaling of the mixed layer enhance export production and the *f*-ratio in the WAP region, particularly in the coast and shelf regions (r^2 = 0.35 for NCP versus MLD, n = 32, p < 0.001), consistent with MLD being a key factor in regulating export production in this region. NCP in the offshore region was generally low regardless of variation of MLD, and associated with low GPP and Chl a in this region. Low offshore NCP is probably also a consequence of severe iron limitation (see section 4.2).

4.2. Influence of Nutrient Supply

4.2.1. Phosphate Uptake and NCP

[55] Depth-integrated phosphate drawdown (ΔP), derived from the method of *Serebrennikova and Fanning* [2004], records the production during the growing season, while our O_2 NCP examines production in the timescale of 1–2 weeks. To make phosphate drawdown comparable to our NCP, we calculate the daily averaged NCP (NCP_{PO4}), based on the part of ΔP in the mixed layer:

$$NCP_{PO4} = \frac{106 \times 1.4 \times \Delta P_{MLD}}{\Delta t} \quad (6)$$

where 106 is the assumed stoichiometric ratio of C:P [*Redfield et al.*, 1963], 1.4 is the O_2:C NCP ratio [*Marra*, 2002], and Δt is the length of the growth season. Since phytoplankton growth in the WAP region usually begins after ice retreat [*Ducklow et al.*, 2007], Δt is estimated by the period from the starting day of ice retreat to the date the samples were collected on a station.

[56] NCP_{PO4} is plotted versus NCP (Figure 5e). In most of the central shelf region, the $NCP_{PO4} \approx$ NCP, indicating that our estimates of NCP are similar to the level of production during the growing season up to the time of sampling. In the offshore and southern inshore regions, NCP_{PO4} was much higher than NCP. This implies that NCP had decreased to a lower level at the time of the cruise, and NCP could be much higher in an earlier stage of the growing season. In the northern shelf and coastal regions, most stations have their $NCP_{PO4} \ll$ NCP. Thus, these regions in Jan. may represent a situation of rapidly rising NCP, or peak NCP, relative to the beginning of the growth season.

[57] Seasonal cycle and spatial pattern of phytoplankton blooms in the WAP region are closely associated with the

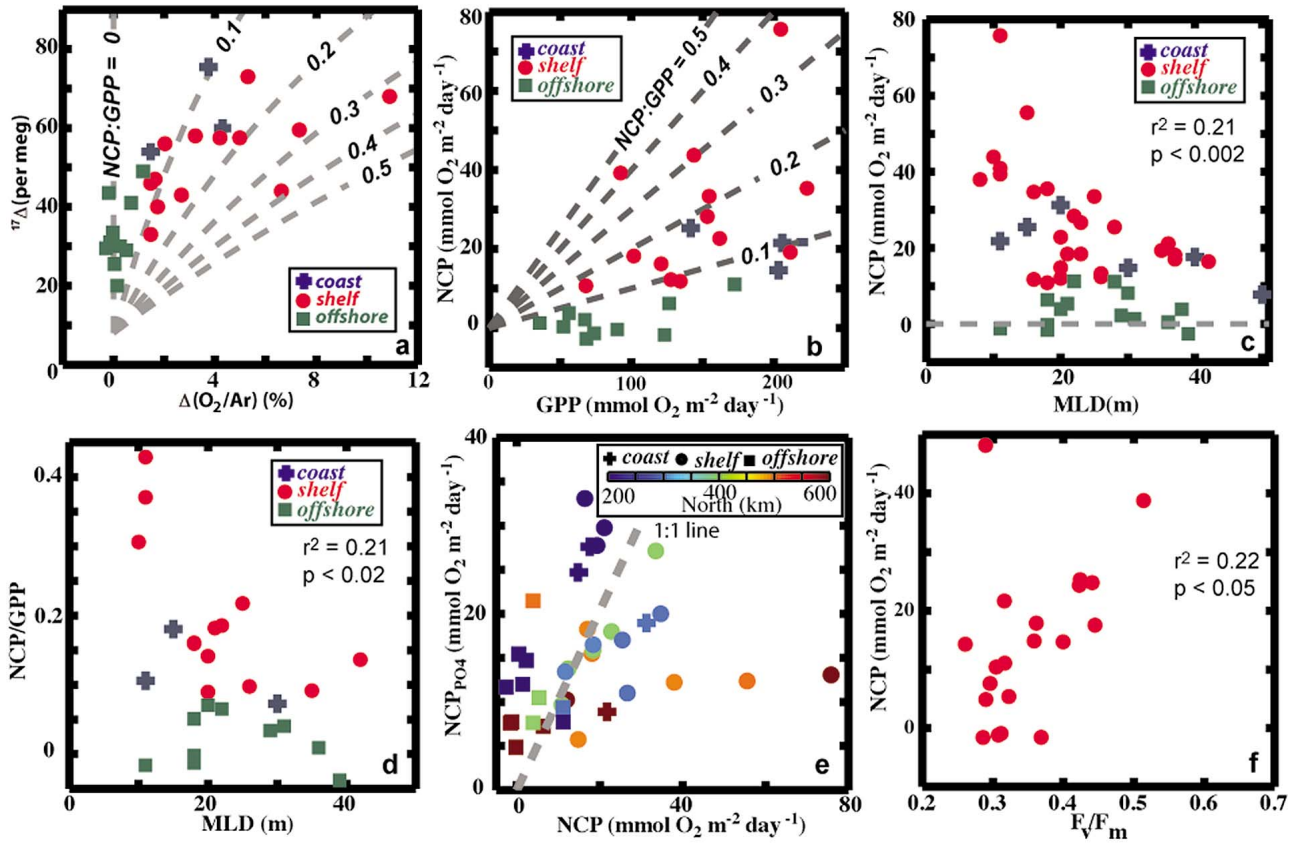

Figure 5. X-Y plots of the results of the correlation studies of (a) $^{17}\Delta$ versus $\Delta(O_2/Ar)$, (b) NCP versus GPP, (c) NCP versus MLD, (d) NCP/GPP versus MLD, (e) daily average NCP (NCP_{PO4}) derived from depth integrated phosphate drawdown versus NCP estimated from the $[O_2]/[Ar]$ ratios, and (f) NCP versus F_v/F_m. Dashed line in Figure 5e is the 1:1 line of NCP_{PO4} and NCP.

sea-ice retreat, and the ice-edge associated blooms usually start in the open sea in October and moves toward the coast as sea-ice retreats [*Smith et al.*, 2008]. Thus, the relationship of NCP_{PO4} and NCP indicates different stages of the growth season from offshore to inshore, and south to north. At the time of the cruise, the southern and offshore regions could be in the situation of a declining bloom, while the northern and inshore regions was probably in the growth or mature stage of a bloom.

4.2.2. Iron and NCP

[58] Iron concentrations are likely to be higher in the coastal and shelf waters than offshore, due to iron supply from both the coast and intrusions of UCDW [*Ducklow et al.*, 2007; *Prézelin et al.*, 2000]. The inferred decrease of iron toward the open sea is thought to account for the inshore-offshore gradient of PP observed in previous studies [*Ducklow et al.*, 2007; *Vernet et al.*, 2008; *Garibotti et al.*, 2003].

[59] The F_v/F_m is used as an indicator of iron limitation in this study. Although F_v/F_m could be affected by various factors such as light, temperature, phytoplankton, nutrient levels [*Cavender-Bares*, 2004] and phytoplankton community structure [*Suggett et al.*, 2004, 2009], iron repletion is observed as the dominant factor that enhances F_v/F_m in the High Nutrient Low Chlorophyll (HNLC) regions of the Southern Ocean [*Boyd et al.*, 1999; *Boyd and Abraham*, 2001; *Strutton et al.*, 1997; *Suggett et al.*, 2009]. As most of our study region resembles the HNLC regions, the spatial variation of F_v/F_m in this region can reflect iron-induced growth stress of phytoplankton.

[60] In our study, F_v/F_m and NCP are positively correlated ($n = 20$, $r^2 = 0.22$, $p < 0.05$), indicating that NCP and export are higher where iron stress of phytoplankton is relieved (Figure 5f). The correlation between F_v/F_m and NCP helps explain the across-shelf decrease of NCP. In the outer-shelf and offshore area, the F_v/F_m ratios are the lowest (around 0.3), and the NCP are low, indicating iron limitation of export production. However, the along-shore decrease of NCP in the coastal area is not tightly associated with F_v/F_m ratios, which were similarly high in the southern and northern coastal region. In iron replete regions, other factors influence NCP.

4.3. Influence of Community Structure

[61] As mentioned in section 3.5, community structure for Jan. 2008 is very similar to that observed in the previous studies. Diatoms dominated the most of the southern region, and cryptophytes dominated the northern coast and inner-shelf region. Chl ain these two groups of phytoplankton account for more than 80% of the total Chl a in the inner-

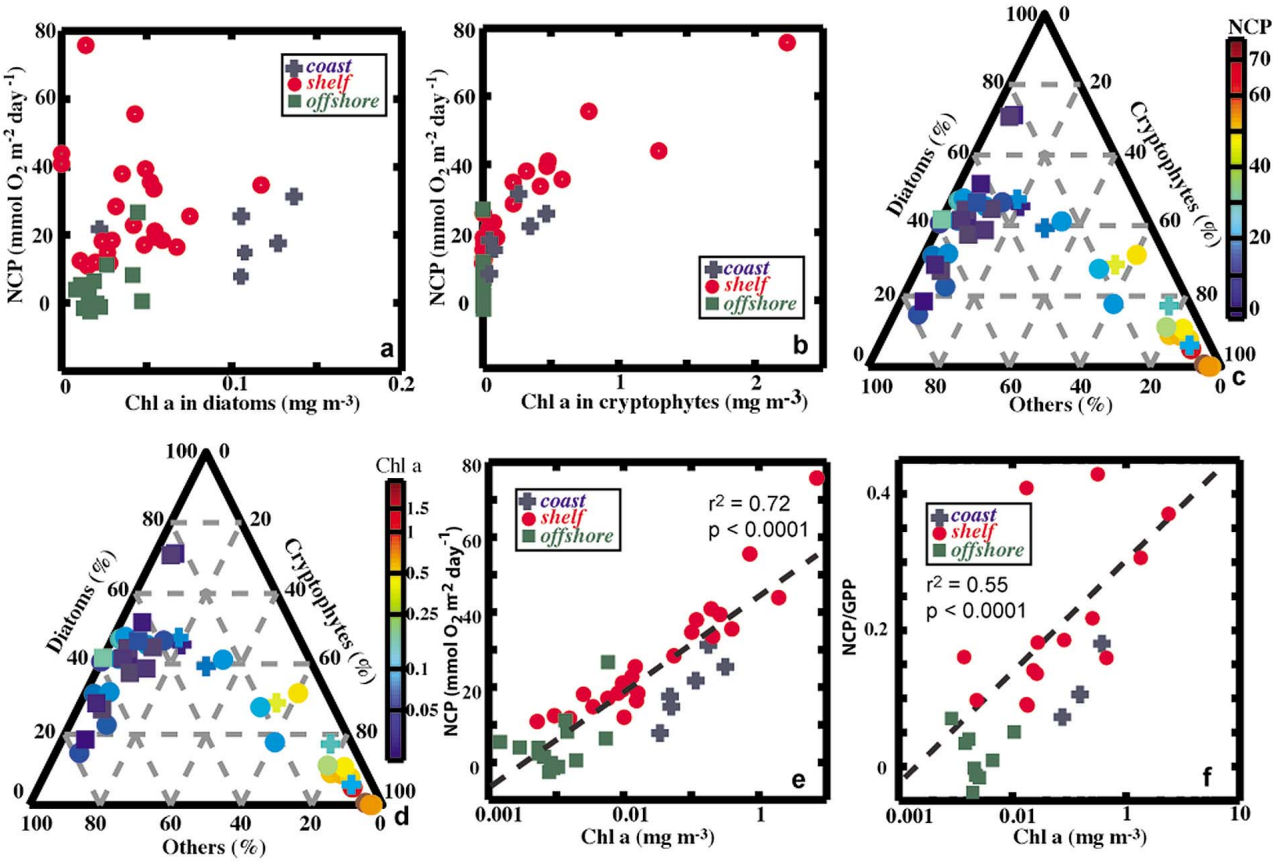

Figure 6. (a) Relationship of NCP with Chl *a* concentration in diatoms. (b) Relationship of NCP with Chl *a* concentration in cryptophytes. (c) Ternary plot showing the contribution of diatoms, cryptophytes and all other examined groups to total Chl *a*. Point closer to the upper corner of the triangle has a higher contribution of diatoms to the total Chl *a*, and point closer to the lower right corner has a higher contribution of cryptophytes. The colors of the circles indicate the magnitude of NCP. (d) The same ternary plot with the colors of the circles showing the magnitude of surface Chl *a* concentration. (e) Relationship of surface Chl *a* concentration with NCP. (f) Relationship of surface Chl *a* concentration with NCP/GPP ratios. Note that the scales of the x-axes in Figures 6e and 6f are logarithmic, and the dashed lines are the regression lines of NCP versus ln(Chl a) and NCP/GPP versus ln(Chl a), respectively.

shelf and coastal regions. Diatoms are usually associated with ice-edge blooms in the region [*Garibotti et al.*, 2003], while cryptophytes are observed to favor fresher, warmer and more strongly stratified water [*Moline et al.*, 2004]. Therefore, the difference in community composition in the coast and inner-shelf region is thought to be a seasonal progression. The diatom-dominated assemblage in the south represents an ice edge community. The cryptophyte-dominated assemblage in the north is a late summer community, where sea-ice retreated earlier after exerting its own influence, and influence of glacier meltwaters became strong [*Garibotti et al.*, 2003].

[62] Diatoms are usually assumed to be the most important taxon in regulating export production in the Southern Ocean [*Boyd and Newton*, 1999; *De La Rocha and Passow*, 2007]. High export production is usually found at places where blooms of diatoms occur [*Buesseler*, 1998]. Our data indicates a complicated correlation between diatoms and NCP (Figure 6a). First, NCP and NCP/GPP in the offshore region was always low (~0), and diatom Chl a concentration (chl_{diat}) in this region was low (<0.05 mg m^{-3}). In the coast and shelf regions, stations with relatively high diatom Chl a concentration coincided with the mid-range of NCP (~10–40 mmol O_2 m^{-2} day^{-1}). At locations where diatoms were less dominant or absent, NCP spanned from the lowest to the highest end of the range. The largest NCP observed in this region all occurred at places of low f_{diat} and low to intermediate level of diatom Chl a concentration.

[63] Places with high NCP and a low fraction of diatoms were dominated by cryptophytes. There is an positive correlation between NCP versus f_{cryp} and NCP versus chl_{cryp} wherever cryptophytes were present (n = 19, r^2 = 0.65 and 0.76, respectively, both have $p < 0.0001$, see Figure 6b). To further exam the influence of the transition between the major phytoplankton groups on NCP and Chl a, we plot the contribution of diatoms, cryptophytes and the sum of all other groups against NCP and Chl a. Total Chl a and NCP increased when diatoms were replaced by cryptophytes, and

reached peak values when the fraction of cryptophytes was larger than 80% of the three groups (Figures 6c and 6d).

[64] The enhancement of NCP from diatom-dominated to cryptophyte-dominated community could be attributed to the alteration of food web, which is regulated by sea-ice and coastal glacier dynamics. Diatoms are the preferred food source for krill [*Haberman et al.*, 2003], while cryptophytes are favored by salps [*Moline et al.*, 2004]. In addition, krill life histories require a period of sea ice cover [*Siegel et al.*, 1990; *Smetacek and Nicol*, 2005; *Quetin and Ross*, 2003] and krill are declining with reductions in sea ice cover along the WAP [*Atkinson et al.*, 2004]. In contrast, sea ice inhibits salp presence and activity [*Siegel and Piatkowski*, 1990; *Loeb et al.*, 1997], and cryptophyte growth is favored later in the season after sea ice retreat and when glacier runoff is near its seasonal maximum. Therefore, the timing of sea-ice retreat, the input of glacier meltwater, and the phytoplankton composition, facilitate high salp-to-krill ratio in the northern coastal and inner-shelf region and lower ratio in the south [*Garibotti et al.*, 2003]. Salps produce large and rapidly sinking fecal pellets [*Bruland and Silver*, 1983].Therefore, the cryptophyte-salp pathway could have a higher efficiency exporting carbon, which might have led to the high NCP and NCP/GPP observed in the northern region. This hypothesis is to be further tested with the zooplankton composition data from the same cruise.

4.4. The Relationship Between NCP and Chl a

[65] One significant and interesting relationship captured by this work is the high correlation of the natural logarithm of surface Chl a with NCP ($n = 43$, $r^2 = 0.72$, $p < 0.0001$, see Figure 6e) and NCP/GPP ($n = 25$, $r^2 = 0.55$, $p < 0.0001$, Figure 6f). Several attempts have been made in previous studies to estimate export production and the f-ratios from phytoplankton biomass and Chl a concentrations [*Baines and Pace*, 1994; *Dunne et al.*, 2005, 2007; *Eppley and Peterson*, 1979; *Laws et al.*, 2000]. The high spatial resolution of our estimates of NCP and NCP/GPP ratios allow us to derive local algorithms in the WAP region.

[66] *Dunne et al.* [2005] concluded, by analyzing a global data set of new or export production, that the *f*-ratio could best be expressed as a function of temperature and the logarithm of average Chl a concentration in the euphotic zone, i.e.

$$pe_r = -0.0101 \times SST + 0.0668 \times ln(Chl_{eu}) + 0.426 \quad (7)$$

where the term Chl_{eu} ($\mu g/L$) stands for the average Chl a concentration in the euphotic zone.

[67] Following the format of the equation given by *Dunne et al.* [2005], we derive following equation to best fit our data:

$$f = 0.1346 ln(Chl_{ML}) + 0.4662 \quad (8)$$

The SST term is ignored here because SST is close to zero in this region. The f-ratio predicted with this equation accounts for 72% of the variance in observed f-ratios. Our equation is not fully comparable to the *Dunne et al.* [2005] equation because our analysis pertains to the mixed layer while theirs pertains to the euphotic zone, and because ours is restricted to one particular ocean ecosystem or province. Nevertheless, the two equations agree closely over most of the chl rangeof our samples. Our equation demonstrates the potential for a local algorithm that converts Chl a concentration measurements to the f-ratio and ^{14}C PP, and calculates NCP from the product.

5. Summary

[68] In this work, we obtained estimates of NCP, GPP and NCP/GPP ratios for January, 2008 at high spatial resolution in the WAP region, and performed correlation studies between NCP(NCP/GPP) and various environmental and ecological properties.

[69] The open ocean region west of the shelf break, and part of the outer-shelf region, is characterized by generally low NCP and NCP/GPP, strong iron limitation, and dominance of prymnesiophytes. NCP can be very low in this region, even when MLD < 20 m. Therefore, iron availability may be the most important factor regulating export production in this region, and distribution of iron might be the main factor that determines the inshore-offshore gradient of GPP, NCP, and community composition.

[70] Export production in the coast and inner-shelf region is generally limited by factors other than iron. The northern area is characterized by high NCP (with the highest NCP occurring in this area), and high iron availability (based on variable fluorescence). It is dominated by cryptophytes. The mixed layer is usually shallow in the region. The compact relationship between NCP and MLD indicates that shallow stratification enhances export production and thus plays a important role in regulating NCP. Input of fresh glacier meltwater, and stratification of the water column, apparently lead to the dominance of cryptophytes, and this could potentially further enhance export production through alteration of the food web.

[71] The southern coast and shelf region presumably have similar levels of iron concentration as the northern. It is distinguished from the northern region by its lower NCP, deeper mixed layer, and the dominance of diatoms. This region may represent an earlier stage in the seasonal succession before the replacement of diatoms by cryptophytes. Low NCP in this region is mainly due to the weaker stratification of the water column, which may also prevent the bloom of cryptophytes.

[72] Diatom blooms can clearly lead to high *f*-ratios and rapid export. However, in our study domain, export was greatest from cryptophyte-dominated communities, presumably due to packaging of organic matter by their grazers.

[73] Overall, our observations and correlation studies indicate that export production is limited by iron, MLD, and community structure in some areas of the study region. During the time of our study, there was a tight relationship between export production and surface Chl a level regardless of changing environmental properties.

[74] **Acknowledgments.** This research was supported by NSF-OPP grant 0823101 to Ducklow and NASA Earth and Space Sciences Fellowship to Huang. We thank all the scientists and the crew on L. M. Gould for collecting samples and making underway measurements, and acknowledge Raytheon Polar Services for assistance with shipboard operations. We are grateful to Bruce Barnett in Bender's lab and Wendy Kozlowski in Vernet's lab for assistance in analyzing samples and processing data. This is Palmer LTER contribution 0386.

References

Angert, A., S. Rachmilevitch, E. Barkan, and B. Luz (2003), Effects of photorespiration, the cytochrome pathway, and the alternative pathway on the triple isotopic composition of atmospheric O_2, *Global Biogeochem. Cycles*, *17*(1), 1030, doi:10.1029/2002GB001933.

Atkinson, A., V. Siegel, E. Pakhomov, and P. Rothery (2004), Long-term decline in krill stock and increase in salps within the Southern Ocean, *Nature*, *432*, 100–103.

Baines, S. B., and M. L. Pace (1994), Relationships between suspended particulate matter and sinking flux along a trophic gradient and implications for the fate of planktonic primary production, *Can. J. Fish. Aquat. Sci.*, *51*(1), 25–36.

Boyd, P. W., and E. R. Abraham (2001), Iron-mediated changes in phytoplankton photosynthetic competence during SOIREE, *Deep Sea Res., Part I*, *48*(11–12), 2529–2550.

Boyd, P., and P. P. Newton (1999), Does planktonic community structure determine downward particulate organic carbon flux in different oceanic provinces?, *Deep Sea Res. I*, *46*, 63–91.

Boyd, P., J. LaRoche, M. Gall, R. Frew, and R. M. L. McKay (1999), Role of iron, light, and silicate in controlling algal biomass in subantarctic waters SE of New Zealand, *J. Geophys. Res.*, *104*, 13,395–13,408.

Bruland, K. W., and M. W. Silver (1983), Sinking rate of fecal pellets from gelatinous zooplankton (salps, pteropods, doliolids), *Mar. Biol.*, *63*, 295–300.

Buesseler, K. O. (1998), The decoupling of production and particulate export in the surface ocean, *Global Biogeochem. Cycles*, *12*(2), 297–310.

Buesseler, K. O., R. T. Barber, M. Dickson, M. R. Hiscock, J. K. Moore, and R. Sambrotto (2003), The effect of marginal ice-edge dynamics on production and export in the Southern Ocean along 170°W, *Deep Sea Res., Part II*, *50*, 579–603.

Buesseler, K. O., A. M. P. McDonnell, O. M. E. Schofield, D. K. Steinberg, and H. W. Ducklow (2010), High particle export over the continental shelf of the west Antarctic Peninsula, *Geophys. Res. Lett.*, *37*, L22606, doi:10.1029/2010GL045448.

Cavender-Bares, J. (2004), From leaves to ecosystems: Using chlorophyll fluorescence to asses photosynthesis and plant function in ecological studies, in *Chlorophyll Fluorescence: A Signature of Photosynthesis*, edited by G. Papageorgiou and Govindjee, pp. 737–755, Kluwer Acad., Dordrecht, Netherlands.

De La Rocha, C. L., and U. Passow (2007), Factors influencing the sinking POC and the efficiency of the biological carbon pump, *Deep Sea Res., II*, *54*, 639–658.

Dierssen, H. M., R. C. Smith, and M. Vernet (2002), Glacial meltwater dynamics in coastal waters west of the Antarctic peninsula, *Proc. Natl. Acad. Sci.*, *99*(4), 1790–1795.

Dong, S., J. Sprintall, S. T. Gille, and L. Talley (2008), Southern Ocean mixed-layer depth from Argo float profiles, *J. Geophys. Res.*, *113*, C06013, doi:10.1029/2006JC004051.

Ducklow, H. W., D. K. Steinberg, and K. O. Buesseler (2001), Upper ocean carbon export and the biological pump, *Oceanography*, *14*(4), 50–58.

Ducklow, H. W., K. Baker, D. G. Martinson, L. B. Quetin, R. M. Ross, R. C. Smith, S. E. Sammerjohn, M. Vernet, and W. Fraser (2007), Marine pelagic ecosystems: The West Antarctic Peninsula, *Philos. Trans. R. Soc. London, Ser. B*, *362*, 67–94.

Ducklow, H. W., M. Erickson, J. Kelly, M. Montes-Hugo, C. A. Ribic, R. C. Smith, S. E. Stammerjohn, and D. M. Karl (2008), Particle export from the upper ocean over the continental shelf of the west Antarctic Peninsula: A long-term record, 1992–2007, *Deep Sea Res., Part II*, *55*(18–19), 2118–2131.

Dunne, J. P., R. A. Armstrong, A. Gnanadesikan, and J. L. Sarmiento (2005), Empirical and mechanistic models for the particle export ratio, *Global Biogeochem. Cycles*, *19*, GB4026, doi:10.1029/2004GB002390.

Dunne, J. P., J. L. Sarmiento, and A. Gnanadesikan (2007), A synthesis of global particle export from the surface ocean and cycling through the ocean interior and on the seafloor, *Global Biogeochem. Cycles*, *21*(4), GB4006, doi:10.1029/2006GB002907.

Eppley, R. W., and B. J. Peterson (1979), Particulate organic-matter flux and planktonic new production in the deep ocean, *Nature*, *282*(5740), 677–680.

Falkowski, P. G., E. A. Laws, R. T. Barber, and J. W. Murray (2003), Phytoplankton, and their role in primary, new and export production, in *Ocean Biogeochemistry*, edited by M. J. R. Fasham, pp. 99–121, Springer, New York.

Fetterer, F. K., W. Meier, and M. Savoie (2007), Sea ice index, http://nsidc.org/, Natl. Snow and Ice Data Cent., Boulder, Colo.

Garibotti, I. A., M. Vernet, M. E. Ferrario, R. C. Smith, R. M. Ross, and L. B. Quetin (2003), Phytoplankton spatial distribution patterns along the western Antarctic Peninsula (Southern Ocean), *Mar. Ecol. Prog. Ser.*, *261*, 21–39.

Haberman, K. L., L. B. Quetin, and R. M. Ross (2003), Diet of the Antarctic krill (*Euphausia superba Dana*): II Selective grazing in mixed phytoplankton assemblages, *J. Exp. Mar. Biol. Ecol.*, *283*(1–2), 97–113.

Hannon, E. P., W. Boyd, M. Silvoso, and C. Lancelot (2001), Modeling the bloom evolution and carbon flows during Soiree: Implications for future in situ iron-enrichments in the southern ocean, *Deep Sea Res., Part II*, *48*, 2745–2774.

Hendricks, M. B., M. L. Bender, and B. A. Barnett (2004), Net and gross O_2 production in the southern ocean from measurements of biological O_2 saturation and its triple isotope composition, *Deep Sea Res., Part I*, *51*, 1541–1561, 2004.

Hidalgo-Gonzalez, R. M., and S. Alvarez-Borrego (2004), Total and new production in the Gulf of California estimated from ocean color data from the satellite sensor SeaWIFS, *Deep Sea Res., Part II*, *51*(6–9), 739–752.

Iverson, R. L., W. E. Esaias, and K. Turpie (2000), Ocean annual phytoplankton carbon and new production, and annual export production estimated with empirical equations and CZCS data, *Global Change Biol.*, *6*(1), 57–72.

Kalnay, E., et al. (1996), The NCEP/NCAR 40-year reanalysis project, *Bull. Am. Meteorol. Soc.*, *77*(3), 437–471.

Klinck, J. M., E. E. Hoffmann, R. C. Beardsley, B. Salihoglu, and S. Howard (2004), Water-mass properties and circulation on the west Antarctic Peninsula Continental Shelf in Austral fall and winter 2001, *Deep Sea Res., Part II*, *51*, 1925–1946.

Kozlowski, W. A. (2008), Pigment derived phytoplankton composition along the western Antarctic Peninsula, Master's thesis, San Diego State Univ., San Diego, Calif.

Kozlowski, W. A., D. Deutschman, I. Garibotti, C. Trees, and M. Vernet (2011), An evaluation of the application of CHEMTAX to Antarctic coastal pigment data, *Deep Sea Res., Part I*, *58*, 350–364.

Laws, E. A. (1991), Photosynthetic quotients, new production and net community production in the open ocean, *Deep Sea Res., Part I*, *38*(1), 143–167.

Laws, E. A., P. G. Falkowski, W. O. Smith, H. Ducklow, and J. J. McCarthy (2000), Temperature effects on export production in the open ocean, *Global Biogeochem. Cycles*, *14*(4), 1231–1246.

Loeb, V., V. Siegel, O. Holm-Hansen, R. Hewitt, W. R. Fraser, W. Z. Trivelpiece, and S. G. Trivelpiece (1997), Effects of sea-ice extent and krill or salp dominance on the Antarctic food web, *Nature*, *387*, 897–900.

Luz, B., and E. Barkan (2000), Assessment of oceanic productivity with the triple-isotope compositoin of dissolved oxygen, *Science*, *288*, 2028–2031.

Luz, B., and E. Barkan (2002), *Tracing mixing in the upper ocean with the three oxygen isotopes*, *Geochim. Cosmochim. Acta*, *66*(15A), A466.

Luz, B., and E. Barkan (2009), Net and gross oxygen production from O_2/Ar, $^{17}O/^{16}O$ and $^{18}O/^{16}O$ ratios, *Aquat. Microb. Ecol.*, *56*, 133–145.

Mackey, D. J., H. W. Higgins, M. D. Mackey, and D. Holdsworth (1998), Algal class abundances in the western equatorial Pacific: Estimation from HPLC measurements of chloroplast pigments using CHEMTAX, *Deep Sea Res., Part I*, *45*, 1441–1468.

Mackey, M. D., D. J. Mackey, H. W. Higgins, and S. W. Wright (1996), CHEMTAX—A program for estimating class abundance for chemical markers: Application to HPLC measurements of phytoplankton, *Mar. Ecol. Prog. Ser.*, *144*, 265–283.

Marra, J. (2002), Approaches to the measurement of plankton production, in *Phytoplankton Productivity: Carbon Assimilation in Marine and Freshwater Ecosystems*, edited by P. J. B. William, D. N. Thomas, and C. S. Reynolds, pp. 78–108, Blackwell, Oxford, U. K.

Martin, J. H. (1990), Glacial-interglacial CO_2 change: The iron hypothesis, *Paleoceanography*, *5*, 1–13.

Martinson, D. G., S. E. Stammerjohn, R. A. Iannuzzi, R. C. Smith, and M. Vernet (2008), Western Antarctic Peninsula physical oceanography and spatio-temporal variability, *Deep Sea Res., Part II*, *55*(18–19), 1964–1987.

Moline, M., H. Claystre, T. Frazer, O. Schofield, and M. Vernet (2004), Alteration of food web along the Antarctic Peninsula in response to a regional warming trend, *Global Change Biol.*, *10*, 1973–1980.

Pollard, R. T., et al. (2009), Southern Ocean deep-water carbon export enhanced by natural iron fertilization, *Nature*, *457*, 577–580.

Prézelin, B. B., E. E. Hoffmann, C. Mengelt, and J. M. Klinck (2000), The linkage between Upper Circumpolar Deep Water (UCDW) and phytoplankton assemblages on the west Antarctic Peninsula continental shelf, *J. Mar. Res.*, *58*, 165–202.

Prézelin, B. B., M. Moline, and J. M. Klinck (2004), Physical forcing of phytoplankton community structure and primary production in continental shelf waters of the western Antarctic Peninsula, *J. Mar. Res.*, *62*, 419–460.

Quay, P. D., S. Emerson, D. O. Wilbur, C. Stump, and M. Knox (1993), The $\Delta^{18}O$ of dissolved O_2 in the surface waters of the sub-Arctic Pacific: A tracer of biological productivity, *J. Geophys. Res.*, *98*(5), 8447–8458.

Quetin, L. B., and R. M. Ross (2003), Episodic recruitment in Antarctic krill, *Euphausia superba*, in the Palmer LTER study region, *Mar. Ecol. Prog. Ser.*, *259*, 185–200.

Redfield, A. C., B. H. Ketchum, and F. A. Richards (1963), The influence of organisms on the composition of sea-water, in *The Sea*, vol. 2, edited by M. N. Hill, pp. 26–77, Wiley Intersci., New York.

Reuer, M. K., B. A. Barnett, M. L. Bender, P. Falkowski, and M. B. Hendricks (2007), New estimates of Southern Ocean biological production rates from O2/Ar ratios and the triple isotope composition of O2, *Deep Sea Res., Part I*, *54*, 951–974.

Serebrennikova, Y. M., and K. A. Fanning (2004), Nutrients in the Southern Ocean GLOBEC region: Variations, water circulation, and cycling, *Deep Sea Res., Part II*, *51*, 1981–2002.

Siegel, V., and U. Piatkowski (1990), Variability in the macrozooplankton community off the Antarctic Peninsula, *Polar Biol.*, *10*, 373–386.

Siegel, V., B. Bergstrom, J. O. Stromberg, and P. H. Schalk (1990), Distribution, size frequencies and maturity stages of krill, *Euphausia superba*, in relation to sea-ice in the northern Weddell Sea, *Polar Biol.*, *10*, 549–557.

Smetacek, V., and S. Nicol (2005), Polar ocean ecosystems in a changing world, *Nature*, *437*, 362–368.

Smith, D. A., E. E. Hofmann, J. M. Klinck, and C. M. Lascara (1999), Hydrography and circulation of the West Antarctic Peninsula Continental Shelf, *Deep Sea Res., Part I*, *46*, 925–949.

Smith, R. C., K. S. Baker, and P. Dustan (1981), Fluorometric techniques for the measurement of oceanic chlorophyll in the support of remote sensing, report, Scripps Inst. of Oceanogr., San Diego, Calif.

Smith, R. C., D. G. Martinson, S. E. Stammerjohn, R. A. Iannuzzi, and K. Ireson (2008), Bellingshausen and western Antarctic Peninsula region: Pigment biomass and sea-ice spatial/temporal distributions and interannual variability, *Deep SeaRes., Part II*, *55*, 1949–1963.

Smith, W. O., and D. M. Nelson (1986), Importance of ice edge phytoplankton production in the Southern Ocean, *Bioscience*, *36*, 251–257.

Stammerjohn, S. E., D. G. Martinson, R. C. Smith, and R. A. Iannuzzi (2008), Sea ice in the western Antarctic Peninsula region: Spatio-temporal variability from ecological and climate change perspectives, *Deep Sea Res., Part II*, *55*(1), 2041–2058.

Strutton, P. G., J. G. Mitchell, J. S. Parslow, and R. M. Greene (1997), Phytoplankton patchiness: Quantifying the biological contribution using fast repetition rate fluorometry, *J. Plankton Res.*, *19*(9), 1265–1274.

Suggett, D. J., H. L. MacIntyre, and R. J. Geider (2004), Evaluation of biophysical and optical determinations of light absorption by photosystem II in phytoplankton, *Limnol. Oceanogr. Methods*, *2*, 316–322.

Suggett, D. J., C. M. Moore, A. E. Hickman, and R. J. Geider (2009), Interpretation of fast repetition rate (FRR) fluorescence: Signature of phytoplankton community structure versus physiological state, *Mar. Ecol. Prog. Ser.*, *376*, 1–19.

Sweeney, C., E. Gloor, A. R. Jacobson, R. M. Key, G. McKinley, J. L. Sarmiento, and R. Wanninkhof (2007), Constraining global air-sea gas exchange for CO_2 with recent bomb ^{14}C measurements, *Global Biogeochem. Cycles*, *21*, GB2015, doi:10.1029/2006GB002784.

Tréguer, P., and G. Jacques (1992), Dynamics of nutrients and phytoplankton, and fluxes of carbon, nitrogen and silicon in the Antarctic Ocean, *Polar Biol.*, *12*, 149–162.

Vernet, M., D. G. Martinson, R. A. Iannuzzi, S. Stammerjohn, W. Kozlowski, K. Sines, R. Smith, and I. Garibotti (2008), Primary production within the sea-ice zone west of the Antarctic Peninsula: I—Sea ice, summer mixed layer, and irradiance, *Deep Sea Res., Part II*, *55*, 2068–2085.

M. L. Bender and K. Huang, Department of Geosciences, Princeton University, Princeton, NJ 08544, USA. (huangk@princeton.edu)

N. Cassar, Division of Earth and Ocean Sciences, Nicholas School of the Environment, Duke University, Durham, NC 27708, USA.

H. Ducklow, The Ecosystems Center, Marine Biological Laboratory, Woods Hole, MA 02543, USA.

M. Vernet, Integrative Oceanography Division, Scripps Institution of Oceanography, University of California, San Diego, La Jolla, CA 92093, USA.